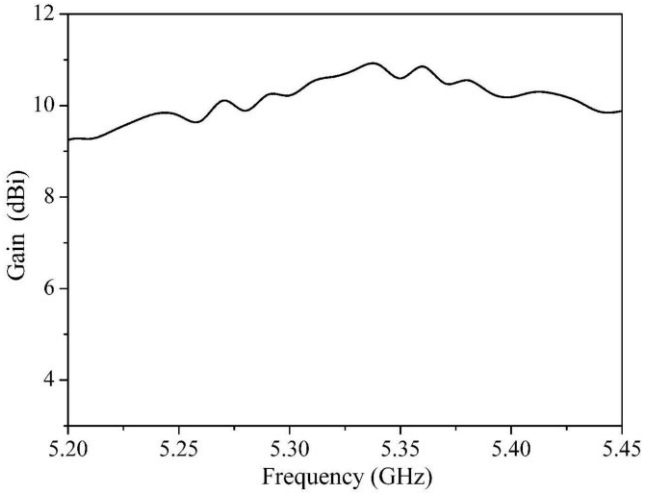

Figure 7 Measured gains of the subarray

3. ARRAY DESIGN

Based on the above element design, a 2 × 2-element DRA subarray with a dimension of 70 × 70 mm^2 is designed, as shown in Figure 3, where the distance between two neighboring elements is selected as $\lambda_0/2$ at 5 GHz and a corporate feed is used to obtain the equal excitation for each element. The photograph of a fabricated 2 × 2-element DRA subarray is shown in Figure 4, and the measured return loss curve with the simulated one is plotted in Figure 5. The measured impedance bandwidth for S_{11} less than −10 dB covers the frequency range of 5.22–5.44 GHz (about 4.2%), which agrees well with the simulated one. The far-field radiation patterns are measured in an anechoic chamber. Figure 6 shows the simulated and measured radiation patterns at *E*- and *H*-planes, in which the half-power beamwidth of radiation pattern in *E*-plane is about 51° with the ratio of front to back is about 15 dB and the radiation in *H*-plane is nearly omni-directional. The corresponding peak gains are also measured comparing with a standard gain horn and shown in Figure 7. The measured peak gain of the 2 × 2-element DRA subarray is 9.4–10.8 dBi across the entire operating frequency band from 5.23 to 5.41 GHz.

4. CONCLUSION

A novel DRA element fed by the microstrip line with an unequal crossstub has been proposed. The simulated results agree well with the experimental ones. The measured impedance bandwidth of the element with the proposed feed is about 4.7%, which is four times of that of the element fed by a microstrip line without any stub. Furthermore, a 2 × 2-element DRA subarray have been designed and measured, which achieves the measured impedance bandwidth of 4.2%, and a gain of 9.4–10.8 dBi in the operating bandwidth. The proposed DRA subarray has a simple structure and a compact size, which is very suitable to large antenna arrays for civilian and military communication applications.

ACKNOWLEDGMENT

This work was supported by the National Natural Science Foundation of China, under Grant No.60571053, and the Shanghai Leading Academic Discipline Project, under Grant No. T0102.

REFERENCES

1. C.S.D. Young and S.A. Long, Wideband cylindrical and rectangular dielectric resonator antennas, IEEE Antennas Wireless Propagat Lett 5 (2006), 426–429.
2. A.A. Kishk, B. Ahn, and D. Kajfez, Broadband stacked dielectric resonator antennas, Electron Lett 25 (1989), 1232–1233.
3. B. Li and K.W. Leung, Strip-fed rectangular dielectric resonator antennas with/without a parasitic patch, IEEE Trans Antennas Propagat 53 (2005), 2200–2207.
4. T.A. Denidni, R. Qinjiang, and A.R. Sebak, Broadband L-shaped dielectric resonator antenna, IEEE Antennas Wireless Propagat Lett 5 (2005), 453–454.
5. G. Drossos, Z.P. Wu, and L.E. Davis, Four-element planar arrays employing probe-fed cylindrical dielectric resonator antennas, Microwave Opt Technol Lett 18 (1998), 315–319.
6. K.W. Leung, H.Y. Lo, K.M. Luk, and E.K.N. Yung, Two-dimensional cylindrical dielectric resonator antenna array, Electron Lett 34 (1998), 1283–1284.
7. A.A. Kishk, Performance of planar four-element array of single-fed circularly polarized dielectric resonator antenna, Microwave Opt Technol Lett 38 (2003), 381–384.

FAST MULTI-FREQUENCY EXTRACTION OF 3D IMPEDANCE BASED ON BOUNDARY ELEMENT METHOD

Wenjian Yu, Changhao Yan, and Zeyi Wang
Department of Computer Science and Technology, Tsinghua University, Beijing 100084, China; Corresponding author: yu-wj@tsinghua.edu.cn

Received 12 December 2007

ABSTRACT: *For the boundary element method used in an impedance extractor FastImp, a scheme to handle the boundary integrals is proposed to accelerate the computation for multiple frequencies. Several techniques are combined in the scheme. The near-field integrals are calculated with a series expansion technique and an approximate formula, whereas the precorrected FFT algorithm is employed for the far-field integrals. Numerical experiments show that the proposed method is several times faster than FastImp for multi-frequency extraction, while preserving high accuracy.* © 2008 Wiley Periodicals, Inc. Microwave Opt Technol Lett 50: 2191–2197, 2008; Published online in Wiley InterScience (www.interscience.wiley.com). DOI 10.1002/mop.23597

Key words: *boundary element method; Helmholtz integral; multi-frequency impedance extraction; series expansion*

1. INTRODUCTION

Because of the skin effect and proximity effect at high frequency, conductor impedance is frequency-dependent, and usually extracted for multiply frequencies. For example, it is necessary to know the impedance for a wide frequency range in the design of RF spiral inductor. Many academic or commercial tools have considered this requirement, with the user command specifying frequency points.

A surface integral formulation [1], also called boundary element method (BEM), was recently proposed for 3D impedance extraction. It was then developed to become a fast wideband solver FastImp, with several efficient numerical techniques employed in [2]. Compared with the well-known partial equivalent element circuit based extractor FastHenry [3], FastImp has several advantages such as avoiding the frequency-dependent discretization of the interior of conductors and substrates, and the capability of full-wave analysis. In FastImp, a precorrected FFT (p-FFT) algorithm separates the integral calculation (i.e. matrix vector product for iterative equation solver) into the far-field and near-field com-

putations, and largely accelerates the former with the FFT scheme. However, FastImp is not efficient enough for the impedance extraction with multiple frequencies. It simply repeats the computation for each single frequency, and costs a lot of time when analyzing a wide frequency range.

Some special techniques referred as "fast frequency-sweep" were proposed to handle the electromagnetic simulation with multiple frequencies [4,5]. However, most of them is based on the finite-element method (FEM), and utilizes the technique of asymptotic waveform evaluation. It is not easy to combine the frequency-sweep techniques with the BEM used in FastImp. A complete multiple reciprocity method (CMRM) was recently proposed to separate the boundary integrals into frequency-dependent and frequency-independent portions, so as to accelerate the multi-frequency impedance extraction based on BEM [6]. However, only magneto-quasistatic (MQS) analysis was considered in [6], and no accelerating approach was employed for solving the final linear system. The approximate formula proposed for far-field integrals will also cause significant error for some actual structures. Therefore, the work in [6] does not result in a practical fast solver for multi-frequency extraction.

In this article, the work in [6] and the p-FFT algorithm are combined together to produce an efficient impedance solver for multiple frequencies. Firstly, the p-FFT algorithm and corresponding division of near-field and far-field integrals are adopted, to accelerate the far-field computations. The CMRM is then presented as a series expansion technique, which decomposes the near-field integral into the frequency-dependent parts and frequency-independent integrals. The latter can be reused among different frequencies. Since the CMRM is only accurate within a window due to numerical issues [6], the near-field integrals outside the window are calculated with the approximate formula or directly, according to a heuristic criterion. Several typical 3D structures are tested to demonstrate the efficiency and robustness of the proposed method. For MQS and full-wave analysis with frequency from 10 MHz to 100 GHz, the error of proposed method to FastImp is less than 0.6%, while it achieves several times speedup for the multi-frequency extraction. Furthermore, a comparison with the frequency-sweep method implemented in HFSS [7] shows that the proposed method is about 10× faster.

2. PRELIMINARIES

2.1. The Boundary Element Method for Impedance Extraction

Ref. [1] proposes a set of surface integral formulae for MQS, electromagneto-quasistatic (EMQS) and full-wave analysis. The boundary integral equation for each conductor domain is:

$$\frac{1}{2}\vec{E}(\vec{y}) = \int_{S_i} G_1(\vec{y},\vec{x})\frac{\partial \vec{E}(\vec{x})}{\partial n_x}dx - \int_{S_i}\frac{\partial G_1(\vec{y},\vec{x})}{\partial n_x}\vec{E}(\vec{x})dx, \quad (1)$$

where $\vec{E}$ is electric field intensity, S_i is the ith conductor surface. For the domain among conductors, the following boundary integral equations hold:

$$-\frac{1}{2}\vec{E}(\vec{y}) = \int_S G_0(\vec{y},\vec{x})\frac{\partial \vec{E}(\vec{x})}{\partial n_x}dx - \int_S \frac{\partial G_0(\vec{y},\vec{x})}{\partial n_x}\vec{E}(\vec{x})dx + \nabla\varphi(\vec{y}), \quad (2)$$

$$\varphi(\vec{y}) = \int_{\bar{S}} G_0(\vec{y},\vec{x})\frac{\rho(\vec{x})}{\varepsilon}dx, \quad (3)$$

where φ is electric potential, and ρ is surface charge density. ε is the permittivity of material, and $\bar{S}$ is the summation of all conductor surfaces. G_0 and G_1 are the Green's function $e^{jkr}/4\pi r$, with different k values. The formulae and values of k are listed in Table 1, where ω is the angular frequency. The k value is calculated under the assumption that frequency is 1 GHz, and the conductor is copper surrounded by air.

With surface discretization and the collocation method [1], the integral equations can be transformed into linear equations. Finally, an overall linear equation system $\boldsymbol{Ax = b}$ is solved. To set up matrix $\boldsymbol{A}$, the major work is computing the coefficients in equations transformed from (1), (2), and (3), which are the integrals with kernel of the Green's function or its derivative:

$$\begin{cases} P_1(a,b) = \displaystyle\int_{\text{panel}_b} G_1(\vec{y}_a,\vec{x})dx = \int_{\text{panel}_b}\frac{e^{jkr(\vec{y}_a,\vec{x})}}{4\pi r(\vec{y}_a,\vec{x})}dx \quad (4) \\ D_1(a,b) = \displaystyle\int_{\text{panel}_b}\frac{\partial G_1(\vec{y}_a,\vec{x})}{\partial n_x}dx = \int_{\text{panel}_b}\frac{\partial}{\delta n_x}\left[\frac{e^{jkr(\vec{y}_a,\vec{x})}}{4\pi r(\vec{y}_a,\vec{x})}\right]dx. \end{cases}$$

Here a and b are panel indexes. panel_b denotes the bth panel, whereas $r(\vec{y}_a,\vec{x})$ stands for the distance between points y_a and x.

In FastImp, the $\boldsymbol{Ax = b}$ is not explicitly generated, and the p-FFT algorithm is used to perform the matrix vector product when solving the equation iteratively. The p-FFT algorithm firstly builds a uniform 3D grid for the whole problem domain. For simplicity, Figure 1 shows a 2D pictorial representation of the grid. A direct stencil, i.e. the 5 × 5 grid with hollow circles in Figure 1, is introduced as a division between the far field and near field. The near-field integral is the interaction between point S and panels within the direct stencil, and is calculated directly. The far-field integral, for example, the integral between panel S and point E, is calculated with the p-FFT scheme.

The p-FFT algorithm can be described as: $A\alpha \rightarrow (D + WHP)\alpha$, which means the matrix vector product $A\alpha$ is calculated as $(\boldsymbol{D}+\boldsymbol{WHP})\alpha$. $\boldsymbol{D}$ is called direct matrix, where only entries

TABLE 1 The Value of Wave Number *k* for Three Extraction Modes

	MQS		EMQS		Full-wave	
	Formula	Value[b]	Formula	Value[a]	Formula	Value[a]
Eq. (1)	$-\sqrt{-i\mu\omega\sigma}$	6.8×10^5	$-\sqrt{-i\mu\omega\sigma}$	6.8×10^5	$-\omega 2\varepsilon\mu - i\omega\mu\sigma$	6.8×105
Eq. (2)	0	0	0	0	$\omega\sqrt{\mu\varepsilon}$	21
Eq. (3)		h		0	$\omega\sqrt{\mu\varepsilon}$	21

[a]For complex number, the value of its norm is listed.

σ and μ are the conductivity and permeability of material, respectively.

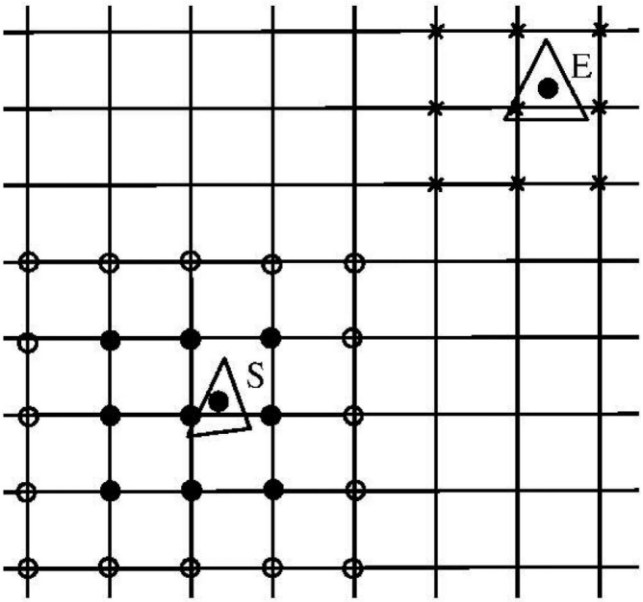

Figure 1 The uniform grid for p-FFT algorithm

corresponding to the near-field integrals are non-zero. $\boldsymbol{W}$ and $\boldsymbol{P}$ are sparse interpolation and projection matrices. $\boldsymbol{H}$ is the convolution matrix, whose product with a vector is computed with FFT [2].

If extracting impedance for multiple frequencies, FastImp firstly generates the p-FFT grid and forms the frequency-independent matrices $\boldsymbol{W}$ and $\boldsymbol{P}$. Then for each frequency point, the matrices $\boldsymbol{D}$ and $\boldsymbol{H}$ are generated, and $\boldsymbol{Ax} = \boldsymbol{b}$ is solved by a preconditioned GMRES solver wherein the p-FFT algorithm is invoked [2]. Generating matrix $\boldsymbol{D}$ needs to calculate the near-field integrals with (4), and is computationally expensive. For example, FastImp spends totally 1820 s to calculate a RF interconnect case, where forming the direct matrix $\boldsymbol{D}$ costs nearly 1444 s [2]. Therefore, reducing the computational time of matrix $\boldsymbol{D}$ is important for improving the BEM-based impedance extraction with multiple frequencies.

2.2. Series Expansion Technique

Without loss of generality, we consider $P_1(a, b)$ in (4) as an example of the frequency-dependent integrals in matrix $\boldsymbol{D}$. According to the Taylor's expansion of e^{jkr}, we have:

$$P_1(a,b) = \int_{\text{panel}_b} \frac{e^{jkr(\vec{y}_a,x)}}{4\pi r(\vec{y}_a,\vec{x})} dx \approx \sum_{i=0}^{2N} (jk)^i \int_{\text{panel}_b} \frac{1}{4\pi r(\vec{y}_a,\vec{x})} \cdot \frac{r(\vec{y}_a,\vec{x})^i}{(i)!} dx. \quad (5)$$

With this formulation, the frequency-dependent integral becomes a linear combination of frequency-independent integrals. For a given structure, these frequency-independent integrals need to be calculated only once, and then can be reused when calculating $P_1(a, b)$ for different k's.

The above series expansion is essentially the soul of CMRM [6]. The convergence of the series is guaranteed, and how to improve the convergence rate is the major concern. Several techniques have been proposed to reduce the numerical difficulty caused by the large variation of r [6]. The actual formula to compute the partial summation of even terms in (5) is:

$$P_1^*(a,b) = \sum_{i=0}^{N} P_{1k,i}^*(a,b) \cdot P_{1r,i}^*(a,b), \quad (6)$$

where

$$P_{1k,i}^*(a,b) = (-1)^i [k r_{\text{avg}}(a,b)]^{2i}, \quad (7)$$

$$P_{1r,i}^*(a,b) = \int_{\text{panel}_b} \frac{1}{4\pi r(\vec{y}_a,\vec{x})} \cdot \frac{r_{rel}(\vec{y}_a,\vec{x})^{2i}}{(2i)!} dx. \quad (8)$$

Here r_{avg} is the average distance between the integral panel vertex and the collocation point, and $r_{\text{rel}}(\vec{y}_a,\vec{x}) = r(\vec{y}_a,\vec{x})/r_{\text{avg}}$.

However, a severe problem still exists, causing large error when evaluating (6). Because of the large variance of frequency and the norm of k in impedance extraction, the norm of kr_{avg} in (7) varies from about 10^{-3} to 10^2. If kr_{avg} is large (for example, larger than (10), the summation in (6) will suffer from severe numerical cancellation. To solve this problem, a window concept was proposed to restrict the formula (6) to the integrals where corresponding kr_{avg} is small [6]. For a specified k (i.e. a specified frequency), a criterion $kr_{\text{avg}}(a,b) < w$, is used to judge if the integral can be calculated by the series expansion. Here w is a non-dimensional value and called relative window size. The critical distance $r_w = w/k$ is obviously dependent on frequency. When frequency f rises, k increases and r_w decreases.

3. REUSE OF THE BOUNDARY INTEGRAL COMPUTATIONS

In this section, two simple observations are firstly presented for improving the reuse of boundary integrals among different frequencies. Then, how to combine the techniques of series expansion and p-FFT is discussed. To revamp the inaccuracy of approximate formula, a heuristic criterion is proposed for the near-field integrals outside the window. Finally, we summarize with the algorithm flow.

3.1. Two Simple Observations

With carefully investigating Table 1, one can find out two ideas for reusing the calculation of matrix $\boldsymbol{D}$. Firstly, the integrals in (2) and (3) for MQS or EMQS analysis are frequency-independent, which should be utilized for the multi-frequency extraction. Secondly, in the full-wave simulation, the integral kernels in (2) and (3) are just the same. Therefore, the integrals in (3) can be directly got from (2) at the same frequency.

The reduction of computational time brought by above observations is usually limited. There are still many arduous frequency-dependent integrals for forming matrix $\boldsymbol{D}$.

3.2. Combine the Series Expansion with the p-FFT Technique

The p-FFT algorithm accelerates the computation in both forming and solving $\boldsymbol{Ax} = \boldsymbol{b}$, and it is robust to guarantee high accuracy [2]. Therefore, we shall combine it with the series expansion technique to ensure efficient solution of $\boldsymbol{Ax} = \boldsymbol{b}$. This combination is explained with Figure 2, where a 3×3 grid is the direct stencil for p-FFT algorithm, and a circle with radius r_w depicts the window wherein the series expansion technique can be used for reusing among different frequencies. An evaluation point at panel center and some scattered panels for calculating integrals are also depicted.

The series expansion technique provides an accurate and reusable scheme of integral calculation for the panels within the window. However, these reusable integrals would not account for

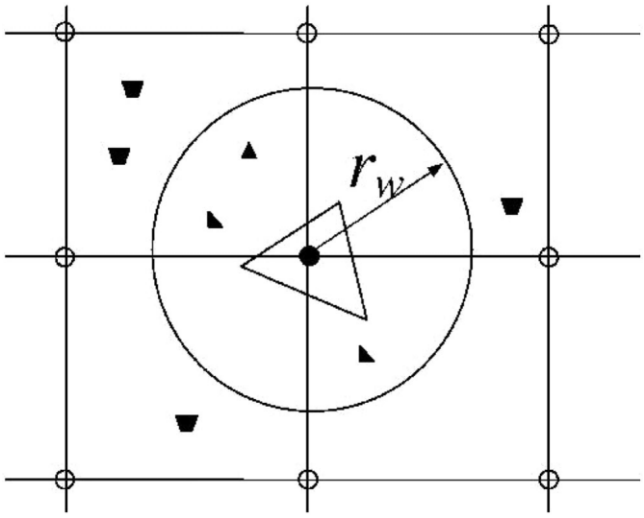

Figure 2 The p-FFT direct stencil and the window for series expansion

a large portion of the near-field integrals when the window size r_w is smaller than the size of direct stencil. This happens for high frequency, or the problem with large panel size. Efficient technique is needed to calculate the near-field integrals outside the window (which are on the quadrilateral panels shown in Fig. 2).

3.3. Calculate the Near-Field Integrals outside the Window

Ref. [6] proposed an approximate integral formula. We use it for the near-field integrals outside the window, and propose a criterion to restrict its usage for the accuracy concern.

Introducing the r_{avg} to (5), we get:

$$P_1(a,b) = \lim_{N\to\infty} \sum_{i=0}^{2N} \frac{(jkr_{avg})^i}{(i)!} \int_{panel_b} \frac{1}{4\pi r(\vec{y}_a,\vec{x})} \cdot r_{rel}(\vec{y}_a,\vec{x})^i dx. \quad (9)$$

If we ignore the variance of $r_{rel}(\vec{y}_a,\vec{x})$ on the panel, i.e., assume it to be 1, (9) can be approximated by:

$$P_1(a,b) \approx \lim_{N\to\infty} \sum_{i=0}^{2N} \frac{(jkr_{avg})^i}{(i)!} \cdot \int_{panel_b} \frac{1}{4\pi r(\vec{y}_a,\vec{x})} dx = e^{jkr_{avg}} \int_{panel_b} \frac{1}{4\pi r(\vec{y}_a,\vec{x})} dx. \quad (10)$$

The formula in (10) includes a frequency-dependent item and a frequency-independent integral, and can be calculated very quickly because the integral term is just the 0th item of $P_{1r,i}{}^*(a,b)$ in (8). This approximate formula is not bothered by numerical issue, either. Similar approximate formula can be obtained for the other kind of integral in (4) [6].

The accuracy of (10) depends on the assumption used. If $r_{rel}(\vec{y}_a,\vec{x})$ has large variance on panel b, the approximate formula will lose accuracy. So, we define a concept of large-variation integral. For this kind of integral, we do not use the approximate formula, and instead calculate it directly. To determine if $P_1(a, b)$ is a large-variation integral, we calculates the relative distances

$$r_{rel}(\vec{y}_a,\vec{x}_{b,j}) = r(\vec{y}_a,\vec{x}_{b,j})/r_{avg}(a,b) \quad (11)$$

at the vertices of panel b (see Fig. 3). If there is any vertex whose relative distance does not fall in an interval $[1-\delta, 1+\delta]$, $P_1(a, b)$ is regarded as a large-variation integral. Otherwise, it can be calculated with (10). The δ is a predefined tolerance value.

Since the imaginary part of k is positive, the $P_1(a, b)$ calculated with (10) has very small value. So, even when the approximate formula induces error to some extent, the accuracy of final result is preserved. With the approximate formula and the heuristic criterion, the number of reusable integrals increases further without loss of accuracy.

3.4. Algorithm Flow

Below is the algorithm flow for impedance extraction with multiple frequencies.

(1) Make panel discretization, build the 3-D p-FFT grid, and calculate frequency-independent matrices $\boldsymbol{W}$ and $\boldsymbol{P}$;

(2) If the analysis mode is MQS or EMQS, calculate and store matrices $\boldsymbol{D}$ and $\boldsymbol{H}$ for Eqs. (2) and (3);

(3) Else calculate and store the frequency-independent integrals in series expansion technique and the approximate formula, for the near-field integrals for Eq. (2);

(4) EndIf;

(5) Calculate and store the frequency-independent integrals in series expansion technique and the approximate formula, for the near-field integrals for Eq. (1);

(6) For each frequency point,

(6.1) If the analysis mode is MQS or EMQS, reuse the $\boldsymbol{D}$ and $\boldsymbol{H}$ matrix from Step 2;

(6.2) Else fill $\boldsymbol{H}$ matrix, and calculate each near-field integral to fill $\boldsymbol{D}$ matrix:

(6.2.1) If the integral is within the window, calculate it with series expansion technique;

(6.2.2) ElseIf the integral is not a large-variation integral, calculate it with the approximate formula;

(6.2.3) Else directly calculate the integral;

(6.2.4) EndIf;

(6.3) EndIf;

(6.4) Prepare the preconditioner for equation solution;

(6.5) Solve $\boldsymbol{Ax = b}$ with preconditioned GMRES solver, where matrix-vector product is performed with p-FFT algorithm;

(6.6) Calculate and output impedance results;

(7) EndFor.

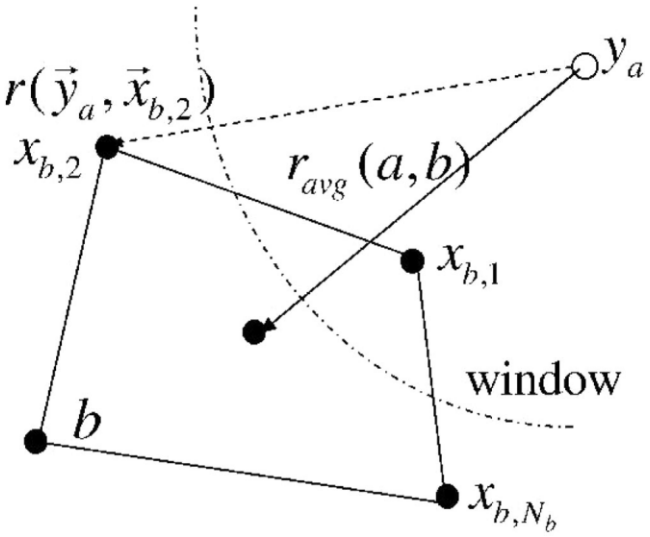

Figure 3 Relative distance for judging the large-variation integral

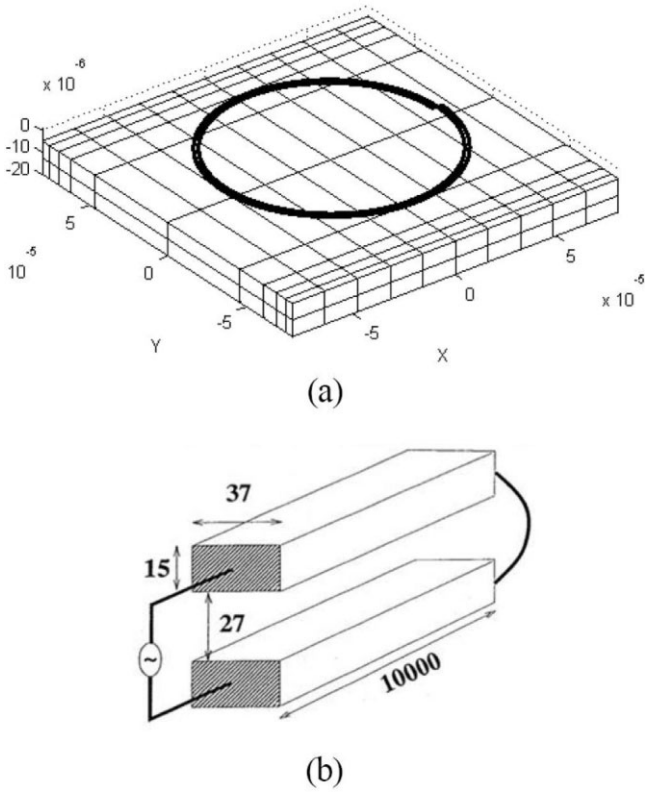

Figure 4 Two examples: (a) spiral inductor over a substrate ground plane, (b) long shorted transmission line

To preserve high accuracy, in the flow there are possibly some near-field integrals calculated directly. To reflect this efficiency loss, we define a concept of hit ratio as follows:

$$R_{\mathrm{h}} = \frac{N_{\mathrm{h}}}{N_{\mathrm{h}} + N_{\mathrm{m}}} \times 100\%, \tag{12}$$

where N_{h} and N_{m} are the numbers of near-field integrals calculated by the proposed techniques and calculated directly, respectively. A 100% R_{h} means the maximum reuse is attained.

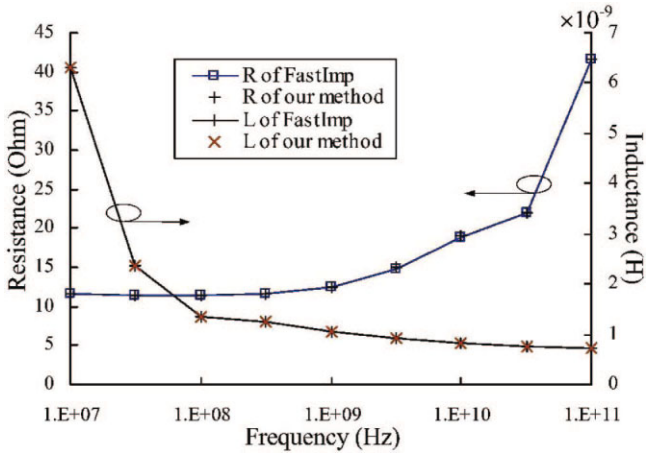

Figure 5 Resistance and inductance of the spiral inductor over a substrate ground plane. [Color figure can be viewed in the online issue, which is available at www.interscience.wiley.com]

4. NUMERICAL RESULTS

We implement the proposed method based on the FastImp Release_v1.0 [8]. The relative window size is set to 2π, and the truncated number $2N$ is 12. The experiments are carried out on a Sun Fire V880 server with 750 MHz CPU.

4.1. Spiral Inductor over a Substrate Ground Plane

The first example is a two-turn spiral inductor above a substrate ground plane, whose geometry is shown in Figure 4(a). The spiral is made of copper, with 100 μm diameter and 1 μm $\times$ 1 μm cross section. The dimension of ground plane is 160 μm $\times$ 160 μm $\times$ 15 μm, whose conductivity is 2.9×10^5 sm^{-1}. The distance between spiral and substrate is 5 μm. We perfrom MQS analysis, with frequency varying from 10 MHz to 100 GHz.

The resistances (R) and inductances (L) calculated by FastImp and our method are shown in Figure 5. The curves from both methods coincide with each other very well on the whole frequency range. The maximum discrepancy between both results is 0.6%, for R at 10 GHz frequency.

Figure 6 shows the accumulative CPU time of FastImp and our method, along with the CPU time for solving $\boldsymbol{Ax} = \boldsymbol{b}$. Because our method does not affect the equation solution in FastImp, its time curve would be parallel to that for equation solution if the computation of generating the coefficient matrix was totally reused. Although this ideal scenario will not happen, Figure 6 shows our method approaches to it very well. The rapider rise of our computational time at frequencies larger than 10 GHz is because the hit ratio R_{h} decreases from 100%. It becomes about 50% when frequency is 100 GHz.

The details of CPU time spent by FastImp and our method, for the first three frequency points, are listed in Table 2. For FastImp, the "frequency-independent part" is the time for filling the matrices $\boldsymbol{W}$ and $\boldsymbol{P}$. For our method, which realizes the kernel $1/r$ used in (2), it includes extra time for generating other matrices (Steps 2 in the algorithm flow). In the frequency-dependent calculation, the most time-consuming operation is filling matrix $\boldsymbol{D}$. From the table we can see, the time for filling matrix $\boldsymbol{D}$ is reduced by **44** times (253.9 s/5.8 s) for the second and later frequencies. Finally, the total CPU time of our method for calculating the nine frequency points is 2056 s, exhibiting a speedup ratio of **2.2** over FastImp.

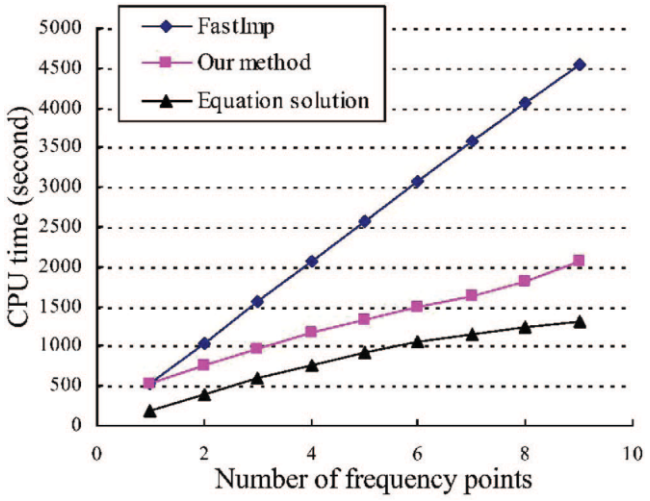

Figure 6 Computational time versus number of frequency points, for the spiral inductor above a ground plane. [Color figure can be viewed in the online issue, which is available at www.interscience.wiley.com]

TABLE 2 The Details of CPU Time Spent by FastImp and Our Method for the First Three Frequency Points (in Second)

	FastImp			Our method		
Frequency point	#1	#2	#3	#1	#2	#3
Frequency-independent part	31.9	–	–	98.4	–	–
Frequency-dependent calculation (Fill D matrix)	301.5 (246.1)	309.3 (253.9)	317.6 (261.7)	239.8 (225.4)	20.8 (5.8)	20.6 (5.8)
Equation solution	190.7	206.6	195.9	193.6	205.5	193.5
Total time	524.2	516.0	513.5	531.8	226.3	214.2

4.2. Long Shorted Transmission Line

This test case is got from [1], and shown in Figure 4(b). The wires are made of copper, with dimensions of 10,000 μm $\times$ 37 μm $\times$ 15 μm for each. We perform full-wave analysis to extract the impedances for frequencies from 1 GHz to 18 GHz. The magnitude and phase of the calculated impedance are plotted in Figure 7, where the curves match those from analytical formula [1]. For this case, the discrepancy between results of our method and FastImp is less than 0.01%.

The accumulative computational times of FastImp and our method are shown in Figure 8. The speedup ratio of our method to FastImp is **3.4**. Because of the large panel size, most near-field integrals for (1) do not fall in the window of series expansion technique. With the approximate formula approach in Section 3.3, the hit ratio R_h is improved to 78%, otherwise it is about 1%. The CPU time for our method without the approximate formula is also plotted in Figure 8. It shows this technique largely improves the efficiency without sacrifice of accuracy.

Because in full-wave analysis the integral kernels in (2) and (3) have much smaller k value (see Table 1), they correspond to larger absolute window size r_w. This guarantees large reusing hit ratio for (2) and (3). From this point of view, our method is very suitable for the full-wave analysis.

4.3. More Discussion and Comparison

The comparisons of the proposed method and FastImp for the two examples are summarized as Table 3, including the numbers of panels and unknowns. Suppose the computational time of FastImp for one frequency is T_0, in which T_d is spent on filling the direct matrix $\boldsymbol{D}$. Then, a rough estimation of the speedup ratio of our method is $T_0/(T_0-T_d)$. If there are sufficient frequency points, and the time of filling $\boldsymbol{D}$ matrix is reduced to be negligible, this estimation can be reached. In Table 3, the estimative and actual speedup ratios are listed. For the first example, the actual value is even slightly larger than the estimation. The reason is that we utilize the frequency-independent property of kernel $1/r$ in (2). More structures including conductor crossover bus and stacked spirals are tested, and the maximum error of proposed method is always less than 1%. Since the ratio T_d/T_0 changes for different test cases, the speedup ratio of our method over FastImp varies from 1.8 to 4.1.

To compare our method with the fast frequency-sweep method, experiments with HFSS, a full-wave solver based on FEM [7], are carried out on a PC with Pentium D 2.8 GHz CPU. The full-wave analysis is performed for the transmission-line example. Under the fast-sweep mode, HFSS spends 3578 seconds CPU time to finish the simulation (excluding the time for adaptive mesh refinement). For a rough comparison, we consider the difference of CPU frequencies and conclude that our method is about **12** times faster than the frequency-sweep method in HFSS. The computational results of HFSS are shown in Figure 9. Since the FEM employed

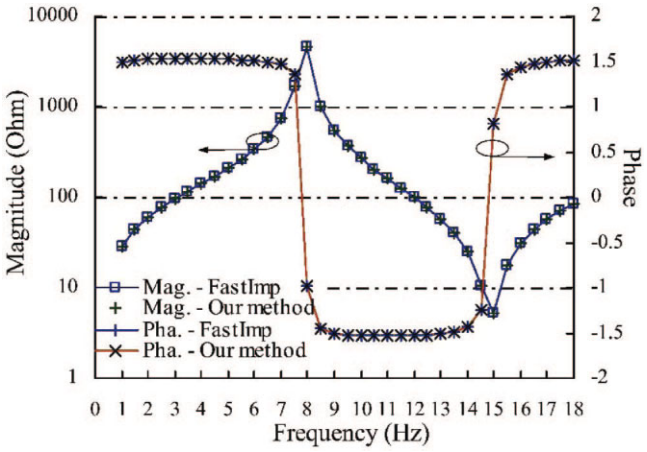

Figure 7 Magnitude and phase of the impedance of the shorted transmission line. [Color figure can be viewed in the online issue, which is available at www.interscience.wiley.com]

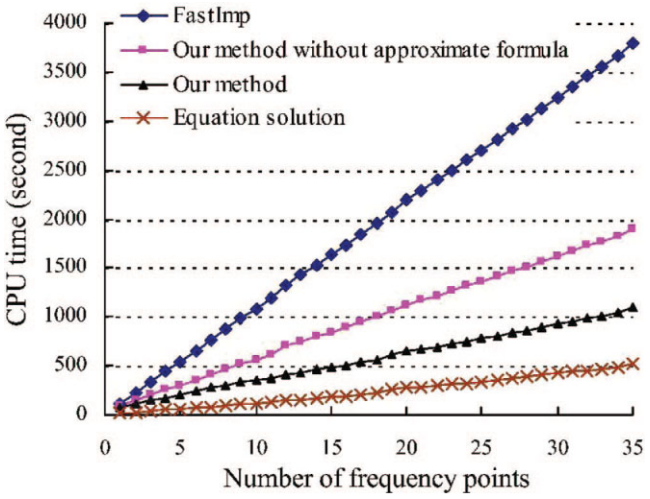

Figure 8 Computational time versus number of frequency points, for the transmission line example. [Color figure can be viewed in the online issue, which is available at www.interscience.wiley.com]

TABLE 3 Summary of the Comparisons for the Two Examples

	Example 1	Example 2
Number of panels	7,498	864
Number of unknowns	52,490	6,916
CPU time of FastImp (s)	4,537	3,793.2
CPU time of our method (s)	2,056	1,104.3
Estimative speedup ratio	2.0	4.1
Actual speedup ratio	2.2	3.4

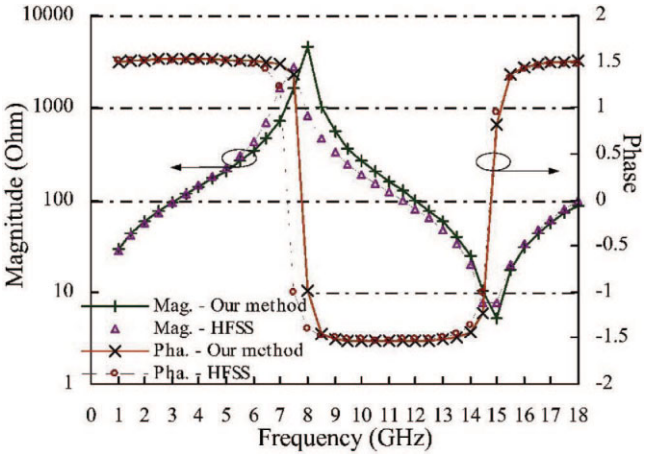

Figure 9 Magnitude and phase of impedance calculated by HFSS and our method. [Color figure can be viewed in the online issue, which is available at www.interscience.wiley.com]

by HFSS makes volume discretization of 3D region, our method based on BEM demonstrates higher efficiency.

5. CONCLUSION

Based on the boundary element method employed by FastImp, techniques for calculating the integrals are presented to improve the efficiency of multiple-frequency extraction. The frequency-dependent near-field integrals are calculated with a series expansion technique and approximate formulae, which enable large computational reuse among different frequencies. Along with the p-FFT algorithm for far-field integrals, the proposed method becomes robust and efficient for multi-frequency impedance extraction. Numerical experiments validate the accuracy and efficiency of the proposed method.

ACKNOWLEDGMENTS

This work was supported by the National Natural Science Foundation of China under Grant 90407004, and 60401010. It was supported in part by the Basic Research Foundation of Tsinghua National Laboratory for Information Science and Technology (TNList).

REFERENCES

1. J. Wang, A new surface integral formulation of EMQS impedance extraction for 3-D structures, Ph.D Dissertation, MIT, Cambridge, MA, 1999.
2. Z. Zhu, B. Song, and J. White, Algorithms in FastImp: A fast and wide-band impedance extraction program for complicated 3-D geometries, IEEE Trans Comput Aided Des 24 (2005),981–998.
3. M. Kamon, M.J. Tsuk, and J. White, FastHenry: A multipole-accelerated 3-D inductance extraction program, IEEE Trans Microw Theor Tech 42 (1994),1750–1758.
4. S.V. Polstyanko, R. Dyczij-Edlinger, and J.-F. Lee, Fast frequency sweep technique for the efficient analysis of dielectric waveguides, IEEE Trans Microw Theor Tech 45 (1997),1118–1126.
5. J. Liu, J.-M. Jin, E.K.N. Yung, and R.S. Chen, A fast, higher order three-dimensional finite-element analysis of microwave waveguide devices, Microw Opt Tech Lett 32 (2002),344–352.
6. C. Yan, W. Yu, and Z. Wang, Application of the complete multiple reciprocity method for 3D impedance extraction with multiple frequency points, Eng Anal Bound Elem 30 (2006),640–649.
7. Ansoft Corporation, HFSS v9.0 user's manual, PA, 2003.
8. Z. Zhu, B. Song, and J. White, FastImp user's guide, Available: http://www.mit.edu/cpg/research_codes.htm

WIDEBAND BANDPASS FILTER USING UNPOWERED HEMT AMPLIFIERS

Yong Kyu Kim and Sung Woo Hwang
Research Center for Time-domain Nano-functional Devices and Department of Electronics and Computer Engineering, Korea University, 5-1, Anam, Sungbuk, Seoul 136-713, Korea;
Corresponding author: swhwang@korea.ac.kr

Received 12 December 2007

ABSTRACT: *A wideband bandpass filter using unpowered, packaged HEMT amplifiers is proposed and implemented. The key idea is to utilize very small parasitic capacitances of the unpowered HEMT as a part of the feedback loop connecting LC resonators. At the input power of −10 dBm, the 3 dB bandwidth of the fabricated bandpass filter is 93.6% of the center frequency (1.536 GHz). Furthermore, our filter does not show appreciable spurious up to 12 GHz. These internal capacitances of the HEMT extracted from the equivalent circuit modeling are shown to be in the range of 10–500 fF.* © 2008 Wiley Periodicals, Inc.

Microwave Opt Technol Lett 50: 2197–2200, 2008; Published online in Wiley InterScience (www.interscience.wiley.com). DOI 10.1002/mop.23623

Key words: *bandpass filters; HEMT; LC filter; feedback; resonators*

1. INTRODUCTION

Wideband bandpass filters, whose bandwidths are larger than 20% of their center frequencies (f_o), are important in many different applications such as radio transceivers, measurement instruments, radar systems, and satellite systems [1–3]. So far, most of the wideband bandpass filters working at GHz frequencies have used microstrip lines. Some examples are using suspended stripline technology [3, 4], quarter wavelength stub microstrips [3, 5], and coplanar waveguides [3, 6]. However, it is cumbersome to fine-tune these microstrip filters so that mass-fabrication of such filters has been difficult. On the other hand, lumped element filters can be easily fine-tuned by simply replacing components. However, wideband lumped element filters in GHz ranges require capacitors with unrealistic capacitance values ranging from several tens of fF to several hundreds of fF. Active filters using active impedance and negative resistance [7] have been demonstrated but, they have high noise figures and narrow bandwidths.

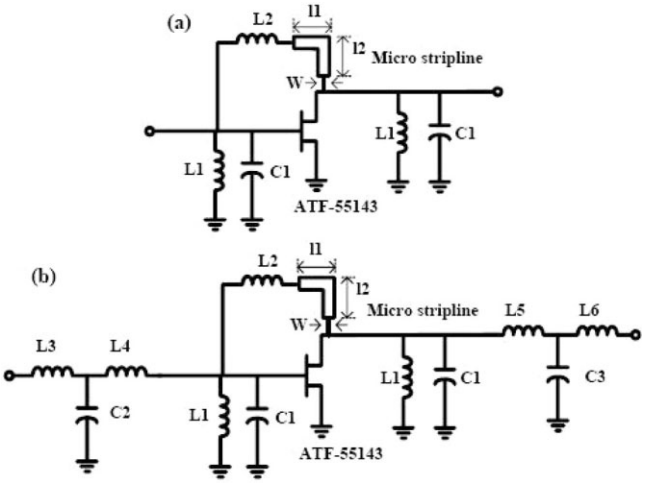

Figure 1 Schematics of (a) the first bandpass filter and (b) the second bandpass filter